

MINISTRY OF NATIONAL DEFENSE
MILITARY TECHNICAL ACADEMY

LE THI THANH HUYEN

REPEATED INDEX MODULATION
FOR OFDM SYSTEMS

Specialization: Electronic Engineering
Specialization code: 9 52 02 03

SUMMARY OF TECHNICAL DOCTORAL THESIS

Ha Noi - 2020

**THIS WORK IS COMPLETED AT MILITARY
TECHNICAL ACADEMY - MINISTRY OF NATIONAL DEFENSE**

Supervisor: Prof. Tran Xuan Nam

Reviewer 1: Assoc. Prof. Le Nhat Thang

Reviewer 2: Assoc. Prof. Tran Duc Tan

Reviewer 3: Assoc. Prof. Nguyen Xuan Quyen

This thesis will be defended in front of the Academy-level Doctoral Examination Board according to the Decision No 1111, April 15, 2020 of the President of Military Technical Academy, meeting at the Military Technical Academy at time ... date ... month ... year

This thesis could be found at:

- National Library of Vietnam
- Library of Military Technical Academy

LIST OF PUBLICATIONS

1. **L. T. T. Huyen**, and T. X. Nam, "Performance Analysis of Repeated Index Modulation for OFDM with MRC Diversity over Nakagami- m Fading Channel," *Journal of Science and Technology*, No.196, pp. 90–102, Feb., 2019.
2. **T.T.H.Le**, X.N.Tran, "Performance Analysis of Repeated Index Modulation for OFDM with MRC and SC diversity Under Imperfect CSI," *AEU - International Journal of Electronics and Communications, (ISI-SCI, Q2, IF=2.853)*, Vol. 107, pp. 199-208, Jul. 2019, <https://doi.org/10.1016/j.aeue.2019.05.022>, Available online 23 May, 2019.
3. **L. T. T. Huyen**, and T. X. Nam, "Performance Analysis of Repeated Index Modulation with Coordinate Interleaving over Nakagami- m Fading Channel," *Research and Development on Information and Communication Technology (RD-ICT) of Journal of Information and Communication Technology*, Vol. 2019, No. 1, pp. 23-30, Jun. 2019.
4. **T. T. H. Le**, V. D. Ngo, M. T. Le, X. N. Tran, "Repeated Index Modulation-OFDM with Coordinate Interleaving: Performance Optimization and Low-Complexity Detectors," *IEEE Systems Journal, (ISI - SCI, Q1, IF=4.463)*, vol. , no. , pp. , 20xx. (Under review).
5. **T. T. H. Le**, and X. N. Tran, "Repeated index modulation for OFDM with space and frequency diversity," *Advanced Technologies for Communications (ATC), 2017 International Conference on. IEEE*, pp. 97–102, Oct., 2017 (Scopus).
6. **T. T. H. Le**, V. D. Ngo, M. T. Le, X. N. Tran, "Repeated Index Modulation with Coordinate Interleaved OFDM," *2018 5th NAFOSTED Conference on Information and Computer Science (NICS)*, pp. 115-119, Nov., 2018 (Scopus).

CONCLUSIONS AND FUTURE WORKS

Achievable results of the thesis

1. This thesis has proposed two systems: the RIM-OFDM system with diversity reception exploits simultaneously the frequency and spatial diversity to achieve better SEP performance than the conventional IM-OFDM with diversity reception; The RIM-OFDM system with CI attains higher reliability and flexibility than the conventional IM-OFDM-CI system.
2. The closed-form expressions for IEP, SEP and BEP were derived to investigate the system performance and provide an insight into the impacts of the system parameters on the performance.
3. The low-complexity detectors were also proposed to reduce the complexity while still achieve nearly same performance of the ML detector.

Future works

1. The proposed RIM-OFDM-MRC/SC system uses ML detector which has high complexity. The proposal of detectors to reduce the complexity of ML could be an interesting topic for future research.
2. The proposal in Chapter 2 is considered for SIMO configuration. In order to further improve the diversity gain and transmission reliability, extending RIM-OFDM to the MIMO and cooperative communication systems is a challenging topic and very attractive for future works.
3. The performance of the RIM-OFDM-CI system in Chapter 3 is investigated under the perfect CSI condition. Evaluating the impacts of channel estimation errors on the system performance is a significantly meaningful topic for future research.
4. The proposals in Chapter 2 and Chapter 3 of the thesis consider the uncoded systems, it is more interesting when evaluating the SEP and BER performance of the system with channel coding.
5. The performance in terms of SEP and BER is analyzed for the two proposed systems. Further analysis using other evaluated parameters would probably give additional insights into the performance of the proposed systems.

INTRODUCTION

1. Background of research

Wireless communication has been considered to be the fastest developing field of the communication industry. Nowadays, the fifth generation (5G) system is expected to be an ubiquitous communication between anybody, anything at anytime with high data rate and transmission reliability, low latency. The 5G system continues employing orthogonal frequency division multiplexing (OFDM) as one of the primary modulation technologies. Meanwhile, based on OFDM, index modulation for OFDM (IM-OFDM) has been proposed and emerged as a promising multi-carrier transmission technique. IM-OFDM uses the indices of active sub-carriers of OFDM systems to convey additional information bits. There are several advantages over the conventional OFDM proved for IM-OFDM such as the reliability, flexibility and the energy efficiency. However, in order to be accepted for possible inclusion in the 5G standards and have a complete understanding about the IM-OFDM capability, more studies should be carried out. This is also a potential research direction that has attracted much attention of researchers.

2. Thesis contributions

1. Proposing and analyzing the performance of a repeated IM-OFDM system with spatial diversity using maximal ratio combination and selection combination (RIM-OFDM-MRC and RIM-OFDM-SC). This system achieves the diversity order of $2L$, double diversity gain compared to the conventional IM-OFDM with diversity reception.
2. Proposing and analyzing the performance of a repeated IM-OFDM system with coordinate interleaving (RIM-OFDM-CI) that achieves better reliability than the conventional IM-OFDM-CI. Based on the performance analysis, proposing a simple method to determine the optimal rotation angle to minimize the error probability. Three low-complexity detectors are proposed for RIM-OFDM-CI to relax the computational complexity.

3. Thesis outline

This thesis includes 90 pages and is organized in three chapters including the introduction, conclusion and references.

Chapter 1

RESEARCH BACKGROUND

1.1 Basic principle of IM-OFDM

Index modulation for OFDM is an OFDM-based transmission technique which utilizes the sub-carrier index to convey more data bits in addition to the M -ary modulation. The incoming data bits in IM-OFDM are divided into two parts. The first part is used to select the indices of active sub-carriers, while the second part is fed to an M -ary mapper as in the conventional OFDM system. However, the IM-OFDM system only activates a subset of sub-carriers, leaving the remaining sub-carriers to be zero padded. Since the information bits are transferred not only by the M -ary modulated symbols but also by the indices of the active sub-carriers, IM-OFDM can attain better transmission reliability and higher energy efficiency than that of the conventional OFDM.

The block diagram of a typical IM-OFDM system is illustrated in Fig. 1.1. The system consists of N_F sub-carriers which are separated into G sub-blocks, each with N sub-carriers. At the transmitter, a sequence of incoming m bits is first separated into G groups of p bits. For the g -th sub-block, the incoming p bits are then split into two bit sequences. The first $p_1 = \lfloor \log_2(C(N, K)) \rfloor$ bits are to select K out of N sub-carriers by using either look-up table or combinational number system.

The second bit sequence of length $p_2 = K \log_2 M$ is to determine the complex modulated symbols that are transmitted over the active sub-carriers. Based on the defined symbols and index set, the IM-OFDM sub-block maps each modulated symbol to the transmitted signal over the corresponding activated sub-carrier as in an example in Table 1.1.

At the receiver, either maximum likelihood (ML) or log-likelihood ratio (LLR) detector is used to jointly detect both active sub-carrier indices and M -ary modulated symbols.

Without taking into account the cyclic prefix (CP), the spectral efficiency of the IM-OFDM system, measured in bit/s/Hz, is given as follows

$$\eta = \frac{\lfloor \log_2(C(N, K)) \rfloor + K \log_2 M}{N}. \quad (1.1)$$

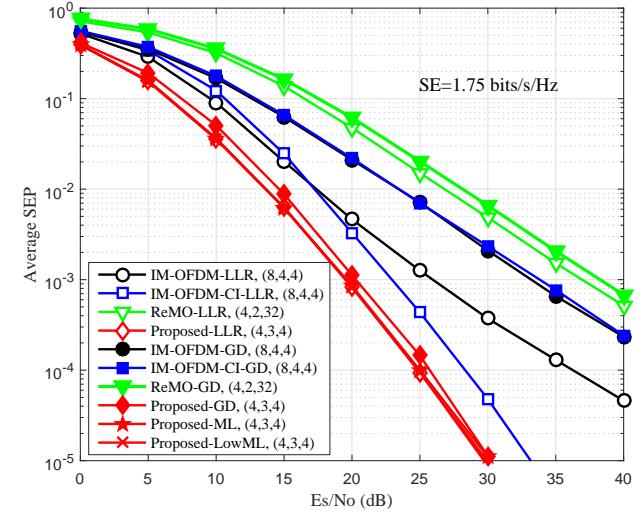


Figure 3.5: SEP performance of RIM-OFDM-CI and benchmark systems using different detectors.

The SEP performance of RIM-OFDM-CI and the reference systems using the ML, LowML, LLR, GD detectors at the same spectral efficiency of 1.75 bits/s/Hz are compared in Fig. 3.5. The proposed scheme using LLR detector outperforms the benchmarks. Particularly, at the SEP of 10^{-3} , RIM-OFDM-CI-LLR provides a gain of about 6 dB, 3.5 dB and 17 dB over IM-OFDM, IM-OFDM-CI and ReMO using LLR detector, respectively. When using LLR and LowML, the proposed scheme also attains the same performance of the ML detector. The proposed system using GD detection also considerably improves the error performance of the benchmark systems.

3.6 Summary of chapter 3

This chapter proposed and analyzed the performance of RIM-OFDM-CI. Based on the theoretical results, the optimal constellation rotation angle has been determined. Three low-complexity detectors that allow the system to reduce detection complexity while enjoying comparable SEP performance with the ML detector have also been proposed.

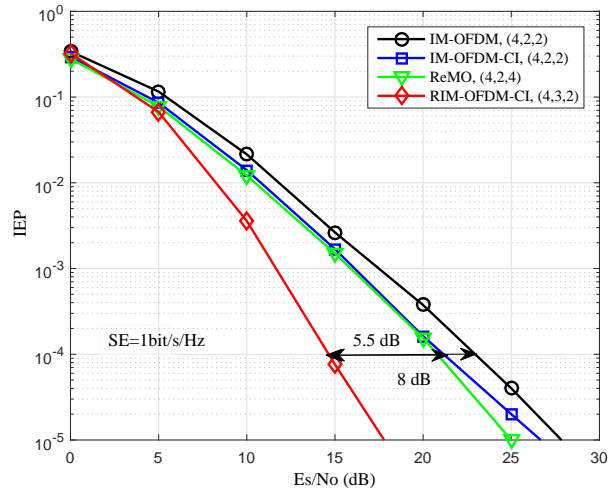


Figure 3.3: Index error performance of RIM-OFDM-CI, IM-OFDM, IM-OFDM-CI and ReMO systems at the spectral efficiency of 1 bit/s/Hz.

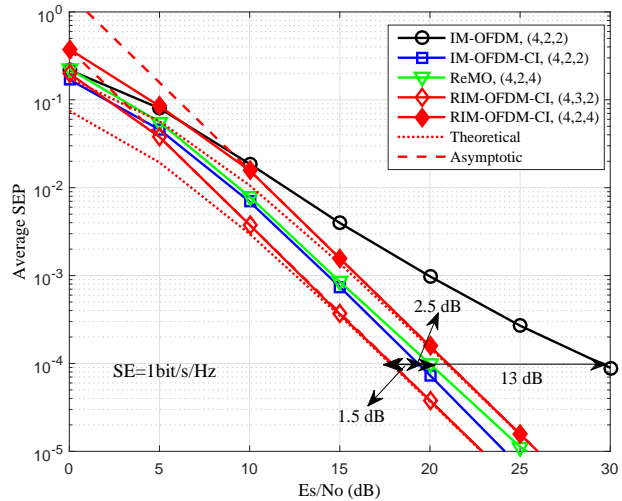
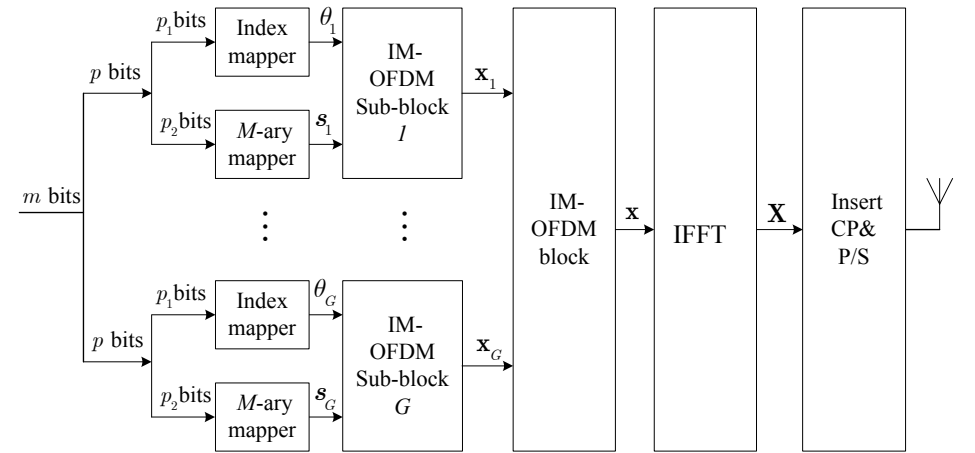
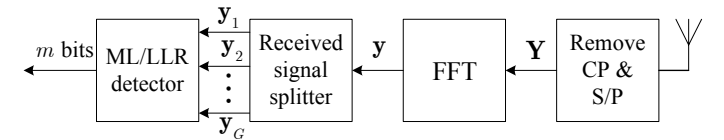


Figure 3.4: SEP performance of RIM-OFDM-CI, IM-OFDM, ReMO and CI-IM-OFDM using ML detection.



(a) IM-OFDM transmitter



(b) IM-OFDM receiver

Figure 1.1: Block diagram of an IM-OFDM system.

1.2 Advantages and disadvantages of IM-OFDM

1.2.1 Advantages:

- IM-OFDM can provide a trade-off between the error performance and spectral efficiency thanks to the adjustable number of active sub-carriers.
- IM-OFDM can achieve improved BER performance over the conventional OFDM system at the same spectral efficiency and the cost of an acceptable detection complexity.
- Since sub-carrier index modulation is conducted for a sub-block g using smaller number of sub-carriers, IM-OFDM is less influenced by the peak-to-average power ratio (PAPR) problem than that of the OFDM system. It is also more robust to inter-carrier interference (ICI) thanks to the activation of only a subset of the available sub-carriers.

Table 1.1: An example of look-up table when $N = 4$, $K = 2$, $p_1 = 2$

<i>Data bits</i>	<i>Indices</i>	<i>Transmitted signal</i>
00	[1, 2]	$[s_\chi, s_\delta, 0, 0]^T$
01	[2, 3]	$[0, s_\chi, s_\delta, 0]^T$
10	[2, 4]	$[0, s_\chi, 0, s_\delta]^T$
11	[1, 3]	$[s_\chi, 0, s_\delta, 0]^T$

1.2.2 Disadvantages:

- The error performance of uncoded/coded IM-OFDM system is generally worse than that of the conventional OFDM system at low SNR regime. This is due to the fact that the index detection is more vulnerable to error under the impact of large noise.
- The detection complexity of the ML detectors for IM-OFDM is higher than that of the conventional OFDM system due to joint estimation of both active indices and the M -ary modulated symbols. This limitation can be facilitated by using the LLR and GD detectors at a slight loss of the transmission reliability.

1.3 Summary

This chapter has introduced the research background of the present thesis. As has been shown, IM-OFDM has several advantages over the conventional OFDM. However, IM-OFDM still suffers from some drawbacks such as the limitation of error performance and high detection complexity. These problems will be addressed in the next chapters.

expressed by the number of floating points (flops) per sub-carrier. The computational complexities of RIM-OFDM-CI using ML, lowML, LLR and GD detectors are estimated and summarized in Table 3.2.

Table 3.2: Complexity of ML, LowML, LLR and GD detectors.

<i>Detector</i>	<i>Number of flops per sub-carrier</i>	(N, K, M) $= (4, 2, 4)$	(N, K, M) $= (8, 4, 8)$
ML	$(30N - 2) cM^{2K}$	7552	974848
LowML	$(2K + 20N + 94MK) c$	3344	203264
LLR	$26MN + 7N + 94MK$	1196	4728
GD	$10N + 94MK$	792	3088

As can be seen from Table 3.2 that the ML detector has the highest complexity in terms of number of flops per sub-carrier, which grows exponentially with M , while those of lowML, GD and LLR detectors are linearly proportional to M . In spite of having the same detection process, the GD detector still can reduce the computational complexity in comparison with the LLR detector.

It can be seen that the complexity of the LLR detector is close to that of the GD when N, K, M are high. Thus, the LLR detector is recommended for large N, K, M since it does not only decrease the computational complexity but also provides the same reliability of the ML detector.

3.5 Performance evaluations and discussions

Fig. 3.3 compares IEP of RIM-OFDM-CI and the benchmark systems at the same spectral efficiency of 1 bit/s/Hz. The proposed scheme has significantly improved IEP performance. Since the proposed scheme employs joint index repetition and coordinate interleaving, it can achieve better diversity gain in the index domain than the IM-OFDM, IM-OFDM-CI and ReMO systems.

Fig. 3.4 depicts the SEP performance of RIM-OFDM-CI, IM-OFDM, IM-OFDM-CI and ReMO systems at the same spectral efficiency of 1 bit/s/Hz. At SEP of 10^{-4} , the proposed scheme provides an SNR gain of about 13 dB, 1.5 dB and 2.5 dB over the IM-OFDM, the IM-OFDM-CI and the ReMO, respectively. This achieved gain is thanks to the improved IEP performance which helps to reduce the M -ary SEP, leading to the overall better error performance compared to the benchmark schemes.

Algorithm 3.2: LLR detection algorithm.

-
- (1) **Input:** $\mathbf{y}_1, \mathbf{y}_2, \mathbf{H}_1, \mathbf{H}_2, \mathcal{S}^\phi, \mathcal{I}$
 - (2) Compute N LLR values $\lambda(\alpha)$ according to (3.19)
 - (3) Find K largest LLR values to estimate $\hat{\theta}$
 - (4) **for** $k = 1$ **to** K **do**
 - (5) Define $\bar{\mathbf{y}}_{\hat{\alpha}_k} = [y_{1\hat{\alpha}_k}^R, y_{1\hat{\alpha}_k}^I, y_{2\hat{\alpha}_k}^R, y_{2\hat{\alpha}_k}^I]^T$
 - (6) Compute $\bar{\mathbf{H}}_{1\hat{\alpha}_k}, \bar{\mathbf{H}}_{2\hat{\alpha}_k}$ according to (3.22)
 - (7) Estimate \hat{a}_k and \hat{b}_k according to (3.23)
 - (8) **end for**
 - (9) **Output:** $\hat{\theta}, \hat{s}_1, \hat{s}_2$
-

3.3.2 GD detector

Algorithm 3.3: GD detection algorithm.

-
- (1) **Input:** $\mathbf{y}_1, \mathbf{y}_2, \mathbf{H}_1, \mathbf{H}_2, \mathcal{S}^\phi, \mathcal{I}$
 - (2) Calculate $\Xi(\alpha) = |y_1(\alpha)|^2 + |y_2(\alpha)|^2$, for $\alpha = 1, \dots, N$
 - (3) Find K highest values of $\Xi(\alpha)$ to detect $\hat{\theta}$
 - (4) **for** $k = 1$ **to** K **do**
 - (5) Define $\bar{\mathbf{y}}_{\hat{\alpha}_k} = [y_{1\hat{\alpha}_k}^R, y_{1\hat{\alpha}_k}^I, y_{2\hat{\alpha}_k}^R, y_{2\hat{\alpha}_k}^I]^T$
 - (6) Compute $\bar{\mathbf{H}}_{1\hat{\alpha}_k}, \bar{\mathbf{H}}_{2\hat{\alpha}_k}$ according to (3.22)
 - (7) Estimate \hat{a}_k and \hat{b}_k according to (3.23)
 - (8) **end for**
 - (9) **Output:** $\hat{\theta}, \hat{s}_1, \hat{s}_2$
-

The GD detector estimates the K indices of active sub-carriers based on K out of N sub-carriers which have the highest power sum of the two groups, i.e., $|y_1(\alpha)|^2 + |y_2(\alpha)|^2$. The estimation of the corresponding M -ary symbols is similar to that of the LLR detector. The GD detection effectively works with the proposed RIM-OFDM-CI system. GD algorithm is given in Table 3.3.

3.4 Complexity Analysis

This section focuses on evaluating the computational complexity of the proposed detectors and comparing them with the ML detector. The complexity is

Chapter 2

REPEATED INDEX MODULATION FOR OFDM WITH DIVERSITY RECEPTION

2.1 RIM-OFDM with diversity reception model

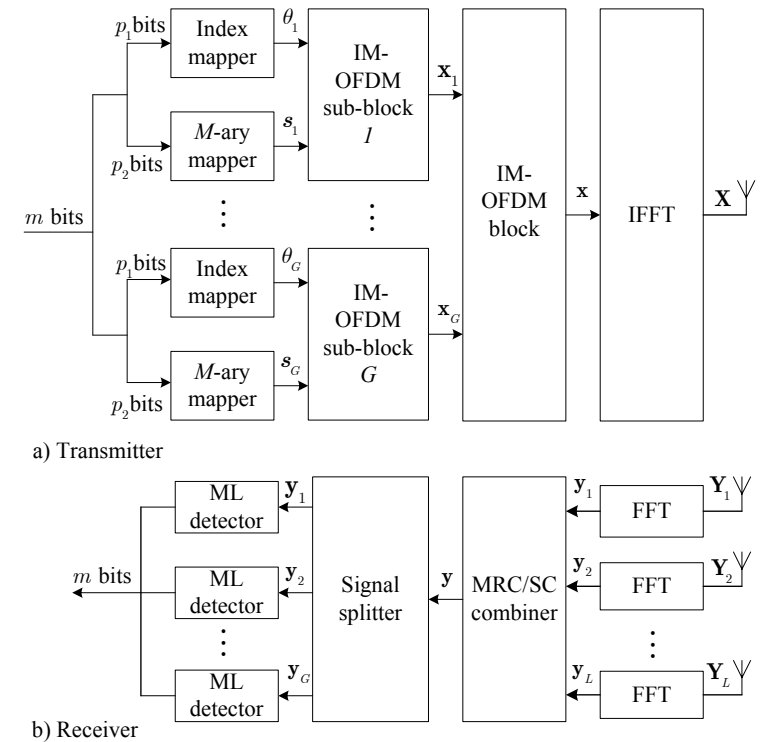


Figure 2.1: Structure of the RIM-OFDM-MRC/SC transceiver.

An up-link SIMO-IM-OFDM system is illustrated in Fig. 2.1. The transmitter is equipped with a single antenna while the receiver has L antennas for diversity reception. Unlike the conventional IM-OFDM, in the proposed system, all active sub-carriers transmit the same M -ary modulated symbol s . The use of this repeated modulation over the sub-carrier domain is to obtain frequency diversity at the cost of spectral efficiency.

At the receiver, either MRC or SC can be used to attain spatial diversity. The output of the reception combiner can be expressed as

$$\mathbf{y} = \mathbf{H}\boldsymbol{\lambda} + \mathbf{n}, \quad (2.1)$$

where $\boldsymbol{\lambda}$ is the index vector, $\mathbf{y} = \{\mathbf{y}_{\text{MRC}}, \mathbf{y}_{\text{SC}}\}$, $\mathbf{H} = \{\mathbf{H}_{\text{MRC}}, \mathbf{H}_{\text{SC}}\}$, $\mathbf{n} = \{\mathbf{n}_{\text{MRC}}, \mathbf{n}_{\text{SC}}\}$, depending on which combiner is used.

2.1.1 RIM-OFDM-MRC

Using a weighted matrix $\mathbf{W} = \mathbf{H}^H$, the output of MRC combiner is given by

$$\mathbf{y}_{\text{MRC}} = \mathbf{H}_{\text{MRC}}\boldsymbol{\lambda} + \mathbf{n}_{\text{MRC}}, \quad (2.2)$$

where $\mathbf{H}_{\text{MRC}} = \mathbf{W}\mathbf{H}$; $\mathbf{n}_{\text{MRC}} = \mathbf{W}\mathbf{n}$.

b) RIM-OFDM-SC

The SC combiner chooses the diversity branch with the largest SNR. The output of the SC combiner is given by

$$\mathbf{y}_{\text{SC}} = \mathbf{H}_{\text{SC}}\boldsymbol{\lambda} + \mathbf{n}_{\text{SC}}, \quad (2.3)$$

where $\mathbf{H}_{\text{SC}} = \text{diag}\{h_{\text{SC}}(1), \dots, h_{\text{SC}}(N)\}$ with each element $h_{\text{SC}}(\alpha) = \max_l |h_l(\alpha)|^2$.

For signal recovery, an ML detector is employed to jointly estimate the index symbols and the M -ary modulated symbol s as follows

$$(\hat{\boldsymbol{\lambda}}, \hat{s}) = \arg \min_{\boldsymbol{\lambda}, s} \|\mathbf{y} - \mathbf{H}\boldsymbol{\lambda} s\|_F^2. \quad (2.4)$$

2.2 Performance analysis under perfect CSI condition

Symbol error probability (SEP), denoted by P_s , is separated into two parts: index symbol error probability P_I and M -ary modulated symbol error probability P_M . Their average values are denoted by \bar{P}_s , \bar{P}_I and \bar{P}_M , respectively.

2.2.1 Performance analysis for RIM-OFDM-MRC

a) Index error probability

Using the pairwise index error probability (PIEP) of the ML detector. PIEP is the probability that the detector mis-detects a transmitted i -th index vector

3.3.1 LLR detector

In order to estimate the indices of active sub-carriers, the LLR detector calculates the following LLR for each sub-carrier as follows

$$\lambda(\alpha) = |y_{1\alpha}|^2 - |y_{1\alpha} - h_{1\alpha}s_\chi|^2 + |y_{2\alpha}|^2 - |y_{2\alpha} - h_{2\alpha}s_\chi|^2, \quad (3.19)$$

where $\alpha = 1, \dots, N$, $s_\chi \in \mathcal{S}^\phi$. Based on N computed LLR values, the LLR detector selects the K largest LLR values to determine the set of active sub-carrier indices.

Upon having successfully detected the indices of active sub-carriers, the corresponding data symbols can be estimated. For each active sub-carrier set $\hat{\theta} = \{\hat{\alpha}_1, \dots, \hat{\alpha}_K\}$, we can express the received signal for active sub-carrier $\hat{\alpha}_k \in \hat{\theta}$, $k = 1, \dots, K$, as follows:

$$\begin{bmatrix} y_{1\hat{\alpha}_k}^R \\ y_{1\hat{\alpha}_k}^I \\ y_{2\hat{\alpha}_k}^R \\ y_{2\hat{\alpha}_k}^I \end{bmatrix} = \begin{bmatrix} h_{1\hat{\alpha}_k}^R & 0 & 0 & -h_{1\hat{\alpha}_k}^I \\ h_{1\hat{\alpha}_k}^I & 0 & 0 & h_{1\hat{\alpha}_k}^R \\ 0 & -h_{2\hat{\alpha}_k}^I & h_{2\hat{\alpha}_k}^R & 0 \\ 0 & h_{2\hat{\alpha}_k}^R & h_{2\hat{\alpha}_k}^I & 0 \end{bmatrix} \times \begin{bmatrix} a_k^R \\ a_k^I \\ b_k^R \\ b_k^I \end{bmatrix} + \begin{bmatrix} n_{1\hat{\alpha}_k}^R \\ n_{1\hat{\alpha}_k}^I \\ n_{2\hat{\alpha}_k}^R \\ n_{2\hat{\alpha}_k}^I \end{bmatrix} \quad (3.20)$$

Equation (3.20) can be rewritten in the vector form as follows:

$$\bar{\mathbf{y}}_{\hat{\alpha}_k} = \bar{\mathbf{H}}_{\hat{\alpha}_k} \bar{\mathbf{s}}_k + \bar{\mathbf{n}}_{\hat{\alpha}_k}, \quad (3.21)$$

where $\bar{\mathbf{H}}_{\hat{\alpha}_k} = [\bar{\mathbf{H}}_{1\hat{\alpha}_k} \quad \bar{\mathbf{H}}_{2\hat{\alpha}_k}]^T$, and $\bar{\mathbf{H}}_{1\hat{\alpha}_k}$, $\bar{\mathbf{H}}_{2\hat{\alpha}_k}$ are respectively given by

$$\bar{\mathbf{H}}_{1\hat{\alpha}_k} = \begin{bmatrix} h_{1\hat{\alpha}_k}^R & 0 \\ h_{1\hat{\alpha}_k}^I & 0 \\ 0 & -h_{2\hat{\alpha}_k}^I \\ 0 & h_{2\hat{\alpha}_k}^R \end{bmatrix}, \quad \bar{\mathbf{H}}_{2\hat{\alpha}_k} = \begin{bmatrix} 0 & -h_{1\hat{\alpha}_k}^I \\ 0 & h_{1\hat{\alpha}_k}^R \\ h_{2\hat{\alpha}_k}^R & 0 \\ h_{2\hat{\alpha}_k}^I & 0 \end{bmatrix}. \quad (3.22)$$

Since columns of channel matrix $\bar{\mathbf{H}}_{\hat{\alpha}_k}$ are orthogonal, data symbols \hat{a}_k and \hat{b}_k can be detected independently by the single-symbol ML detector as follows:

$$\begin{aligned} \hat{a}_k &= \arg \min_{a_k \in \mathcal{S}^\phi} \left\| \bar{\mathbf{y}}_{\hat{\alpha}_k} - \bar{\mathbf{H}}_{1\hat{\alpha}_k} \begin{bmatrix} a_k^R \\ a_k^I \end{bmatrix} \right\|_F^2, \\ \hat{b}_k &= \arg \min_{b_k \in \mathcal{S}^\phi} \left\| \bar{\mathbf{y}}_{\hat{\alpha}_k} - \bar{\mathbf{H}}_{2\hat{\alpha}_k} \begin{bmatrix} b_k^R \\ b_k^I \end{bmatrix} \right\|_F^2. \end{aligned} \quad (3.23)$$

Based on estimated symbols \hat{a}_k and \hat{b}_k , $k = 1, \dots, K$, the symbol vectors for each cluster is recovered as in (3.18). The LLR detection algorithms can be summarized as follows

a final decision on the indices of active sub-carriers which corresponds to the best estimated symbols by

$$\hat{j} = \arg \min_j \{D_j\}, \quad (3.16)$$

where $D_j = \|\mathbf{y}_1 - \mathbf{H}_1 \hat{\mathbf{x}}_{1,j}\|_F^2 + \|\mathbf{y}_2 - \mathbf{H}_2 \hat{\mathbf{x}}_{2,j}\|_F^2$. Using \hat{j} the estimated set of active sub-carrier indices is given by $\hat{\theta} = \theta_{\hat{j}}$. The M -ary modulated symbols of both clusters are then detected as follows

$$\hat{a}_k = \hat{a}_{k,\hat{j}}, \quad \hat{b}_k = \hat{b}_{k,\hat{j}}. \quad (3.17)$$

Based on estimated symbols \hat{a}_k and \hat{b}_k , where $k = 1, \dots, K$, the symbol vectors for each cluster are given by

$$\hat{\mathbf{s}}_1 = [\hat{a}_1 \ \hat{a}_2 \ \dots \ \hat{a}_K]^T, \quad \hat{\mathbf{s}}_2 = [\hat{b}_1 \ \hat{b}_2 \ \dots \ \hat{b}_K]^T. \quad (3.18)$$

The low-complexity ML detection algorithm is summarized as follows:

Algorithm 3.1: Low-complexity ML detection algorithm.

-
- (1) **Input:** $\mathbf{y}_1, \mathbf{y}_2, \mathbf{H}_1, \mathbf{H}_2, \mathcal{S}^\phi, \mathcal{I}$
 - (2) **for** $j = 1$ **to** 2^{p_1} **do**
 - (3) **for** $k = 1$ **to** K **do**
 - (4) Define $(\bar{\mathbf{y}}_{\alpha_k})_j = [y_{1\alpha_k}^R \ y_{1\alpha_k}^I \ y_{2\alpha_k}^R \ y_{2\alpha_k}^I]_j^T$
 - (5) Calculate $(\bar{\mathbf{H}}_{1\alpha_k})_j, (\bar{\mathbf{H}}_{2\alpha_k})_j$ as in (3.14)
 - (6) Estimate $\hat{a}_{k,j}$ and $\hat{b}_{k,j}$ according to (3.15)
 - (7) **end for**
 - (8) From $\hat{a}_{k,j}$ and $\hat{b}_{k,j}$, create $\tilde{\mathbf{s}}_{1,j}, \tilde{\mathbf{s}}_{2,j}$
 - (9) Combine $\tilde{\mathbf{s}}_{1,j}, \tilde{\mathbf{s}}_{2,j}$ and θ_j to generate $\hat{\mathbf{x}}_{1,j}, \hat{\mathbf{x}}_{2,j}$
 - (10) Compute $D_j = \sum_{i=1}^2 \|\mathbf{y}_i - \mathbf{H}_i \hat{\mathbf{x}}_{i,j}\|_F^2$, for $i = 1, 2$
 - (11) **end for**
 - (12) Estimate $\hat{j} = \arg \min_{j=1, \dots, 2^{p_1}} D_j$
 - (13) Generate $\hat{\theta} = \theta_{\hat{j}}, \hat{a}_k = \hat{a}_{k,\hat{j}}, \hat{b}_k = \hat{b}_{k,\hat{j}}$
 - (14) $\hat{\mathbf{s}}_1, \hat{\mathbf{s}}_2$ as in (3.18)
 - (15) **Output:** $\hat{\theta}, \hat{\mathbf{s}}_1, \hat{\mathbf{s}}_2$
-

It can be seen that unlike the ML detector, the proposed lowML detector has the computational complexity of $\sim \mathcal{O}(2^{p_1} MK)$, which linearly increases with M .

into the j -th index vector. The PIEP can be expressed as

$$P(\boldsymbol{\lambda}_i \rightarrow \boldsymbol{\lambda}_j) = Q\left(\sqrt{\frac{\varphi E_s \|\mathbf{H}\boldsymbol{\lambda}_i - \mathbf{H}\boldsymbol{\lambda}_j\|_F^2}{2N_0}}\right), \quad (2.5)$$

where $\boldsymbol{\lambda}_i$ and $\boldsymbol{\lambda}_j$ are transmitted and the estimated index vectors, respectively.

Then, applying the MGF and union bound, the average PIEP of RIM-OFDM-MRC can be obtained as

$$\begin{aligned} \bar{P}_I^{\text{MRC}} &\approx \frac{\vartheta}{12} \left[\mathcal{M}_{\gamma_{\Sigma}^{\text{MRC}}}\left(-\frac{1}{4}\right) + 3\mathcal{M}_{\gamma_{\Sigma}^{\text{MRC}}}\left(-\frac{1}{3}\right) \right] \\ &\approx \frac{\vartheta}{12} \left[\frac{4^{2L}}{(4+\bar{\gamma})^{2L}} + \frac{3^{2L+1}}{(3+\bar{\gamma})^{2L}} \right], \end{aligned} \quad (2.6)$$

where $\vartheta = \sum_{i=1}^c \eta_i / c$.

b) M -ary modulated symbol error probability

The instantaneous SEP of the M -ary modulated symbol is given by

$$\bar{P}_M^{\text{MRC}} \approx 2Q\left(\sqrt{2\gamma_{\Sigma,\alpha}^{\text{MRC}}} \sin(\pi/M)\right), \quad (2.7)$$

Using MGF approach, the average M -ary modulated SEP of RIM-OFDM-MRC is given by

$$\bar{P}_M^{\text{MRC}} \approx \frac{1}{6} \left[\frac{1}{(1+\rho\bar{\gamma})^{LK}} + \frac{3}{(1+\frac{4\rho\bar{\gamma}}{3})^{LK}} \right]. \quad (2.8)$$

As a result, the average SEP of the RIM-OFDM-MRC system is given by

$$\bar{P}_s^{\text{MRC}} \leq \frac{\vartheta}{24} \left[\frac{16^L}{(4+\bar{\gamma})^{2L}} + \frac{3^{2L+1}}{(3+\bar{\gamma})^{2L}} \right] + \frac{1}{12} \left[\frac{1}{(1+\rho\bar{\gamma})^{LK}} + \frac{3}{(1+\frac{4\rho\bar{\gamma}}{3})^{LK}} \right]. \quad (2.9)$$

2.2.2 Performance analysis for RIM-OFDM-SC

a) Index error probability

Using similar method as in RIM-OFDM-MRC, PIEP of RIM-OFDM-SC is given by

$$\bar{P}_I^{\text{SC}} \leq \frac{\vartheta}{12} \left[\mathcal{M}_{\gamma_{\Sigma}^{\text{SC}}}\left(-\frac{1}{4}\right) + 3\mathcal{M}_{\gamma_{\Sigma}^{\text{SC}}}\left(-\frac{1}{3}\right) \right] = \frac{\vartheta}{12} L^2 \left(\bar{P}_{I_1}^{\text{SC}} + 3\bar{P}_{I_2}^{\text{SC}} \right), \quad (2.10)$$

where $\bar{P}_{I_1}^{\text{SC}}$ and $\bar{P}_{I_2}^{\text{SC}}$ are given as follows

$$\bar{P}_{I_1}^{\text{SC}} = \left[\sum_{l=0}^{L-1} \binom{L-1}{l} \frac{4(-1)^l}{4l+4+\bar{\gamma}} \right]^2, \quad \bar{P}_{I_2}^{\text{SC}} = \left[\sum_{l=0}^{L-1} \binom{L-1}{l} \frac{3(-1)^l}{3l+3+\bar{\gamma}} \right]^2. \quad (2.11)$$

b) M -ary modulated symbol error probability

Similar to (2.8), SEP of the M -ary modulated symbol of the RIM-OFDM-SC system is given by

$$\bar{P}_M^{\text{SC}} \approx \frac{L^K}{6} (\bar{P}_{M_1}^{\text{SC}} + 3\bar{P}_{M_2}^{\text{SC}}), \quad (2.12)$$

where $\bar{P}_{M_1}^{\text{SC}}$ and $\bar{P}_{M_2}^{\text{SC}}$ are defined by

$$\bar{P}_{M_1}^{\text{SC}} = \left[\sum_{l=0}^{L-1} \binom{L-1}{l} \frac{(-1)^l}{l+1+\rho\bar{\gamma}} \right]^K, \quad \bar{P}_{M_2}^{\text{SC}} = \left[\sum_{l=0}^{L-1} \binom{L-1}{l} \frac{3(-1)^l}{3l+3+4\rho\bar{\gamma}} \right]^K. \quad (2.13)$$

As a result, the closed-form expression for the average SEP of RIM-OFDM-SC is obtained as follows

$$\bar{P}_s^{\text{SC}} \approx \frac{\vartheta L^2}{24} (\bar{P}_{I_1}^{\text{SC}} + 3\bar{P}_{I_2}^{\text{SC}}) + \frac{L^K}{12} (\bar{P}_{M_1}^{\text{SC}} + 3\bar{P}_{M_2}^{\text{SC}}). \quad (2.14)$$

Where $\bar{P}_{I_1}^{\text{SC}}$, $\bar{P}_{I_2}^{\text{SC}}$, $\bar{P}_{M_1}^{\text{SC}}$, $\bar{P}_{M_2}^{\text{SC}}$ are determined in (2.11), (2.13), respectively.

2.3 Performance analysis under imperfect CSI condition

2.3.1 Performance analysis for RIM-OFDM-MRC

Practically, channel estimation errors can occur at the receiver. The receiver utilizes the actually estimated channel matrix in place of the perfect \mathbf{H} in (2.1) to detect the transmitted signals.

a) Index error probability

Using the similar method as in the case of perfect CSI, the closed-form expression for the average PIEP of RIM-OFDM-MRC under the imperfect CSI condition is given by

$$\bar{P}_I^{\text{MRC}} \leq \frac{\vartheta}{12} \left[\left(\frac{4+2\bar{\gamma}\epsilon^2}{4+\bar{\gamma}+\bar{\gamma}\epsilon^2} \right)^{2L} + 3 \left(\frac{6+3\bar{\gamma}\epsilon^2}{6+2\bar{\gamma}+\bar{\gamma}\epsilon^2} \right)^{2L} \right], \quad (2.15)$$

where ϵ^2 is the error variance.

3.3 Low-complexity detectors for RIM-OFDM-CI

For each possible combination of $\theta = \{\alpha_1, \dots, \alpha_K\}$, which is represented by θ_j , where $j = 1, \dots, 2^{p_1}$, $\theta_j \in \mathcal{J}$, we can express the received signal for sub-carrier $\alpha_k \in \theta_j$, where $k = 1, \dots, K$, as follows

$$\begin{aligned} \begin{bmatrix} y_{1\alpha_k}^R \\ y_{1\alpha_k}^I \\ y_{2\alpha_k}^R \\ y_{2\alpha_k}^I \end{bmatrix}_j &= \begin{bmatrix} h_{1\alpha_k}^R & 0 & 0 & -h_{1\alpha_k}^I \\ h_{1\alpha_k}^I & 0 & 0 & h_{1\alpha_k}^R \\ 0 & -h_{2\alpha_k}^I & h_{2\alpha_k}^R & 0 \\ 0 & h_{2\alpha_k}^R & h_{2\alpha_k}^I & 0 \end{bmatrix}_j \\ &\times \begin{bmatrix} a_k^R \\ a_k^I \\ b_k^R \\ b_k^I \end{bmatrix} + \begin{bmatrix} n_{1\alpha_k}^R \\ n_{1\alpha_k}^I \\ n_{2\alpha_k}^R \\ n_{2\alpha_k}^I \end{bmatrix}_j \end{aligned} \quad (3.12)$$

Equation (3.12) can be rewritten as

$$(\bar{\mathbf{y}}_{\alpha_k})_j = (\bar{\mathbf{H}}_{\alpha_k})_j \bar{\mathbf{s}}_k + (\bar{\mathbf{n}}_{\alpha_k})_j, \quad (3.13)$$

where $(\bar{\mathbf{H}}_{\alpha_k})_j = [(\bar{\mathbf{H}}_{1\alpha_k})_j \ (\bar{\mathbf{H}}_{2\alpha_k})_j]^T$, $(\bar{\mathbf{H}}_{1\alpha_k})_j$ and $(\bar{\mathbf{H}}_{2\alpha_k})_j$ are respectively given by

$$(\bar{\mathbf{H}}_{1\alpha_k})_j = \begin{bmatrix} h_{1\alpha_k}^R & 0 \\ h_{1\alpha_k}^I & 0 \\ 0 & -h_{2\alpha_k}^I \\ 0 & h_{2\alpha_k}^R \end{bmatrix}_j, \quad (\bar{\mathbf{H}}_{2\alpha_k})_j = \begin{bmatrix} 0 & -h_{1\alpha_k}^I \\ 0 & h_{1\alpha_k}^R \\ h_{2\alpha_k}^R & 0 \\ h_{2\alpha_k}^I & 0 \end{bmatrix}_j. \quad (3.14)$$

Since the orthogonal property exists for the columns of channel matrix $(\bar{\mathbf{H}}_{\alpha_k})_j$, the single-symbol ML detector can be used to independently estimate $\hat{a}_{k,j}$ and $\hat{b}_{k,j}$ as follows

$$\begin{aligned} \hat{a}_{k,j} &= \arg \min_{a_k \in \mathcal{S}_\phi} \left\| (\bar{\mathbf{y}}_{\alpha_k})_j - (\bar{\mathbf{H}}_{1\alpha_k})_j \begin{bmatrix} a_k^R & a_k^I \end{bmatrix}^T \right\|_F^2, \\ \hat{b}_{k,j} &= \arg \min_{b_k \in \mathcal{S}_\phi} \left\| (\bar{\mathbf{y}}_{\alpha_k})_j - (\bar{\mathbf{H}}_{2\alpha_k})_j \begin{bmatrix} b_k^R & b_k^I \end{bmatrix}^T \right\|_F^2. \end{aligned} \quad (3.15)$$

Upon having the results from (3.15), the coordinate interleaving principle is applied to each pair of $(\hat{a}_{k,j}, \hat{b}_{k,j})$ to create $\tilde{\mathbf{s}}_1, \tilde{\mathbf{s}}_2$. Then, $\tilde{\mathbf{s}}_1, \tilde{\mathbf{s}}_2$ and θ_j are combined to generate $N \times 1$ symbol vectors $\hat{\mathbf{x}}_{i,j}$. The lowML detector will make

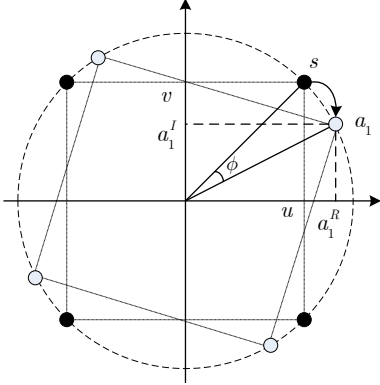


Figure 3.2: Rotated signal constellation.

3.2.2 Optimization of rotation angle

This section introduced a solution to determine the optimum value of the rotation angle, denoted by ϕ_{opt} , to minimize the SEP based on the above performance analysis without utilizing computer search. For simplicity, we only analyze in detail the case of quadrature amplitude modulation (QAM) constellation with $M = 4$ as shown in Fig. 3.2. Following this figure, the imaginary and real parts of the data symbol after phase rotation can be presented as follows

$$\begin{aligned} a_1^R &= u \cos \phi + v \sin \phi, \\ a_1^I &= -u \sin \phi + v \cos \phi. \end{aligned} \quad (3.9)$$

Besides, from above performance analysis, the minimization of SEP becomes the minimization of the value of J function given by

$$J = \sum_{\hat{a}_1 \neq a_1} P(a_1 \rightarrow \hat{a}_1). \quad (3.10)$$

At the high SNR regime, J can be approximated as

$$J \approx \left(\frac{2}{\sin^2 2\phi} + \frac{1}{4 \cos^2 2\phi} \right) \frac{1}{\gamma^2}. \quad (3.11)$$

After some straight mathematical manipulations, the optimum rotation angle for 4-QAM scheme can be calculated as $\phi_{\text{opt}} = 30^\circ$. Applying the similar process, the following optimum values can be determined: $\phi_{\text{opt}} = \{45^\circ, 30^\circ, 9.5^\circ, 40^\circ, 30^\circ\}$ for $M = \{2, 4, 8, 16, 64\}$, respectively.

b) M -ary modulated symbol error probability

The M -ary SEP for RIM-OFDM-SC in the case of imperfect CSI is given by

$$\tilde{P}_M^{\text{MRC}} \approx \frac{1}{6} \left[\frac{1}{\left(1 + \frac{(1-\epsilon^2)\bar{\gamma}\rho}{1+\bar{\gamma}\epsilon^2}\right)^{LK}} + \frac{3}{\left(1 + \frac{4(1-\epsilon^2)\bar{\gamma}\rho}{3(1+\bar{\gamma}\epsilon^2)}\right)^{LK}} \right]. \quad (2.16)$$

Accordingly, the average SEP of RIM-OFDM-MRC under the imperfect CSI condition is obtain as

$$\begin{aligned} \tilde{P}_s^{\text{MRC}} &\approx \frac{\vartheta}{24} \left[\left(\frac{4 + 2\bar{\gamma}\epsilon^2}{4 + \bar{\gamma} + \bar{\gamma}\epsilon^2} \right)^{2L} + 3 \left(\frac{6 + 3\bar{\gamma}\epsilon^2}{6 + 2\bar{\gamma} + \bar{\gamma}\epsilon^2} \right)^{2L} \right] \\ &+ \frac{1}{12} \left[\frac{1}{\left(1 + \frac{(1-\epsilon^2)\bar{\gamma}\rho}{1+\bar{\gamma}\epsilon^2}\right)^{LK}} + \frac{3}{\left(1 + \frac{4(1-\epsilon^2)\bar{\gamma}\rho}{3(1+\bar{\gamma}\epsilon^2)}\right)^{LK}} \right]. \end{aligned} \quad (2.17)$$

2.3.2 Performance analysis for RIM-OFDM-SC

a) Index error probability

The approximated PIEP of RIM-OFDM-SC under the imperfect CSI condition is given by

$$\tilde{P}_I^{\text{SC}} \leq \frac{\vartheta}{12} \left[\mathcal{M}_{\bar{\gamma}\Sigma^{\text{SC}}} \left(\frac{-1}{4 + 2\bar{\gamma}\epsilon^2} \right) + 3\mathcal{M}_{\bar{\gamma}\Sigma^{\text{SC}}} \left(\frac{-2}{6 + 3\bar{\gamma}\epsilon^2} \right) \right] = \frac{\vartheta}{12} L^2 \left(\tilde{P}_{I_1}^{\text{SC}} + 3\tilde{P}_{I_2}^{\text{SC}} \right), \quad (2.18)$$

where $\tilde{P}_{I_1}^{\text{SC}}$, $\tilde{P}_{I_2}^{\text{SC}}$ is given as follows

$$\begin{aligned} \tilde{P}_{I_1}^{\text{SC}} &= \left[\sum_{l=0}^{L-1} \binom{L-1}{l} \frac{(4 + 2\bar{\gamma}\epsilon^2) (-1)^l}{(4 + 2\bar{\gamma}\epsilon^2) l + 4 + \bar{\gamma} + \bar{\gamma}\epsilon^2} \right]^2, \\ \tilde{P}_{I_2}^{\text{SC}} &= \left[\sum_{l=0}^{L-1} \binom{L-1}{l} \frac{(6 + 3\bar{\gamma}\epsilon^2) (-1)^l}{(6 + 3\bar{\gamma}\epsilon^2) l + 6 + 2\bar{\gamma} + \bar{\gamma}\epsilon^2} \right]^2. \end{aligned} \quad (2.19)$$

b) M -ary modulated symbol error probability

Similar to (2.12), the M -ary modulated SEP for RIM-OFDM-SC in the case of imperfect CSI can be approximated by

$$\tilde{P}_M^{\text{SC}} \approx \frac{L^K}{6} (\tilde{P}_{M_1}^{\text{SC}} + 3\tilde{P}_{M_2}^{\text{SC}}), \quad (2.20)$$

where $\tilde{P}_{M_1}^{\text{SC}}$ and $\tilde{P}_{M_2}^{\text{SC}}$ are respectively given by

$$\tilde{P}_{M_1}^{\text{SC}} = \left[\sum_{l=0}^{L-1} \binom{L-1}{l} \frac{(-1)^l}{l+1 + \frac{\rho(1-\epsilon^2)\tilde{\gamma}}{1+\tilde{\gamma}\epsilon^2}} \right]^K, \quad \tilde{P}_{M_2}^{\text{SC}} = \left[\sum_{l=0}^{L-1} \binom{L-1}{l} \frac{3(-1)^l}{3l+3 + \frac{4\rho(1-\epsilon^2)\tilde{\gamma}}{1+\tilde{\gamma}\epsilon^2}} \right]^K. \quad (2.21)$$

At a result, the average SEP of RIM-OFDM-SC under imperfect CSI condition is given by

$$\tilde{P}_s^{\text{SC}} \approx \frac{L^2 \sum_{i=1}^c \eta_i}{24c} (\tilde{P}_{I_1}^{\text{SC}} + 3\tilde{P}_{I_2}^{\text{SC}}) + \frac{L^K}{12} (\tilde{P}_{M_1}^{\text{SC}} + 3\tilde{P}_{M_2}^{\text{SC}}), \quad (2.22)$$

where $\tilde{P}_{I_1}^{\text{SC}}$, $\tilde{P}_{I_2}^{\text{SC}}$, and $\tilde{P}_{M_1}^{\text{SC}}$, $\tilde{P}_{M_2}^{\text{SC}}$ are given in (2.19) and (2.21), respectively.

2.4 Performance evaluation and discussion

2.4.1 Performance evaluation under perfect CSI

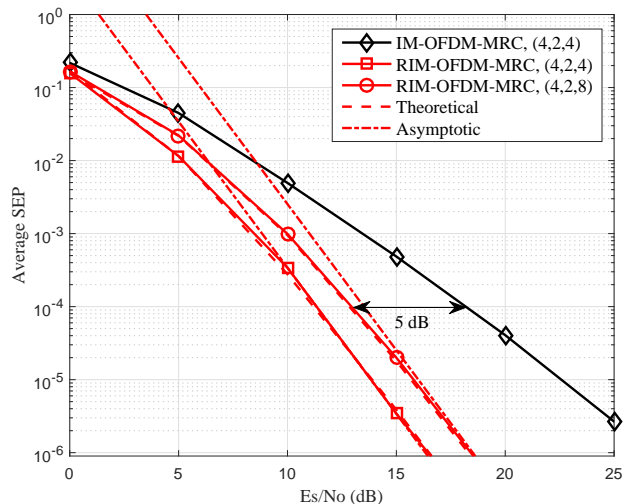


Figure 2.2: The SEP comparison between RIM-OFDM-MRC and the conventional IM-OFDM-MRC system when $N = 4$, $K = 2$, $L = 2$, $M = \{4, 8\}$.

Fig. 2.2 illustrates the comparison between SEP performance of RIM-OFDM-MRC and IM-OFDM-MRC at the spectral efficiency of 1 and 1.25 bits/s/Hz. The proposed system outperforms the reference system. Particularly, at SEP

3.2 Performance analysis

3.2.1 Symbol error probability derivation

Symbol error probability (SEP) of the RIM-OFDM-CI system is given by

$$P_s = \frac{P_I + KP_M}{K+1}, \quad (3.4)$$

where P_I and P_M denote the index error and M -ary modulated symbol error probabilities, respectively. SEP of the M -ary modulated data symbols in RIM-OFDM-CI can be calculated by utilizing the pair-wise error probability (PEP) of modulated symbols. PEP is determined by the probability that a transmitted symbol a_1 is made wrong estimation by symbol \hat{a}_1 .

The conditional PEP of RIM-OFDM-CI can be computed as follows

$$\begin{aligned} P(a_1 \rightarrow \hat{a}_1 | h_1, h_2) &= \Pr [|\tilde{y}_1 - |h_1| \hat{a}_1^R - j |h_2| \hat{a}_1^I|^2 < |\tilde{y}_1 - |h_1| a_1^R - j |h_2| a_1^I|^2 = |\tilde{n}_1|^2] \\ &= Q \left(\sqrt{\frac{|h_1|^2 \Delta_R^2 + |h_2|^2 \Delta_I^2}{2N_0}} \right) \\ &= Q \left(\sqrt{\frac{\tilde{\gamma}_1 \Delta_R^2 + \tilde{\gamma}_2 \Delta_I^2}{2}} \right), \end{aligned} \quad (3.5)$$

where $\Delta_R^2 = |a_1^R - \hat{a}_1^R|^2$ and $\Delta_I^2 = |a_1^I - \hat{a}_1^I|^2$.

Following the MGF approach, the average PEP of the M -ary modulated data symbol is calculated as follows

$$\begin{aligned} P(a_1 \rightarrow \hat{a}_1) &= \frac{\mathcal{M}_\Omega(-\frac{1}{2})}{12} + \frac{\mathcal{M}_\Omega(-\frac{2}{3})}{4} \\ &= \frac{1}{12 \left(1 + \frac{\tilde{\gamma} \Delta_R^2}{4}\right) \left(1 + \frac{\tilde{\gamma} \Delta_I^2}{4}\right)} + \frac{1}{4 \left(1 + \frac{\tilde{\gamma} \Delta_R^2}{3}\right) \left(1 + \frac{\tilde{\gamma} \Delta_I^2}{3}\right)}. \end{aligned} \quad (3.6)$$

Using the union bound, the M -ary modulated SEP is given by

$$P_M = \frac{1}{|S^\phi|} \sum_{a_1 \in S^\phi} \sum_{\hat{a}_1 \neq a_1} P(a_1 \rightarrow \hat{a}_1). \quad (3.7)$$

The approximate average SEP of the repeated IM-OFDM-CI can be obtained as follows

$$P_s \approx \Psi \left[\frac{1}{12 \left(1 + \frac{\tilde{\gamma} \Delta_R^2}{4}\right) \left(1 + \frac{\tilde{\gamma} \Delta_I^2}{4}\right)} + \frac{1}{4 \left(1 + \frac{\tilde{\gamma} \Delta_R^2}{3}\right) \left(1 + \frac{\tilde{\gamma} \Delta_I^2}{3}\right)} \right], \quad (3.8)$$

where $\Psi = K/(K+1)$.

cluster for $N = 4$, $K = 2$, $p_I = 2$ is presented in Table 3.1.

Table 3.1: Example of LUT for $N = 4$, $K = 2$, $p_I = 2$.

p_I	θ	\mathbf{x}_1^T	\mathbf{x}_2^T
00	[1, 2]	$[a_1^R + jb_1^I \ a_2^R + jb_2^I \ 0 \ 0]$	$[b_1^R + ja_1^I \ b_2^R + ja_2^I \ 0 \ 0]$
01	[2, 3]	$[0 \ a_1^R + jb_1^I \ a_2^R + jb_2^I \ 0]$	$[0 \ b_1^R + ja_1^I \ b_2^R + ja_2^I \ 0]$
10	[2, 4]	$[0 \ a_1^R + jb_1^I \ 0 \ a_2^R + jb_2^I]$	$[0 \ b_1^R + ja_1^I \ 0 \ b_2^R + ja_2^I]$
11	[1, 3]	$[a_1^R + jb_1^I \ 0 \ a_2^R + jb_2^I \ 0]$	$[b_1^R + ja_1^I \ 0 \ b_2^R + ja_2^I \ 0]$

It can be seen that the real and imaginary parts of the original M -ary symbols are transferred over different sub-carriers, leading to an improvement of the diversity gain. Combining the index repetition and the joint coordinate interleaving allows RIM-OFDM-CI to activate an arbitrary number of sub-carriers which makes RIM-OFDM-CI more flexible than the conventional IM-OFDM-CI system.

The IM-OFDM sub-block creator receives \mathbf{x}_1 and \mathbf{x}_2 to generate the transmitted vector per sub-block that is given by $\mathbf{x} = [\mathbf{x}_1^T \ \mathbf{x}_2^T]^T$. Under the flat fading channel, the received signal in the frequency domain can be expressed as

$$\mathbf{y} = \mathbf{H}\mathbf{x} + \mathbf{n}, \quad (3.1)$$

where $\mathbf{y} = [y_1 \ y_2]^T$, $\mathbf{H} = \begin{bmatrix} \mathbf{H}_1 & \mathbf{0} \\ \mathbf{0} & \mathbf{H}_2 \end{bmatrix}$ and $\mathbf{n} = [n_1^T \ n_2^T]^T$.

The spectral efficiency of the RIM-OFDM-CI system is given by

$$\eta = \frac{\lfloor \log_2(C(N, K)) \rfloor + 2K \log_2 M}{2N} \quad [\text{bits/s/Hz}]. \quad (3.2)$$

In order to detect the transmitted signal, the receiver employs an ML detector to jointly estimate the active indices and the corresponding data symbols for both clusters. The ML detection for RIM-OFDM-CI is given by

$$(\hat{\theta}, \hat{s}_1, \hat{s}_2) = \arg \min_{\theta, s_1, s_2} \|\mathbf{y} - \mathbf{H}\mathbf{x}\|_F^2. \quad (3.3)$$

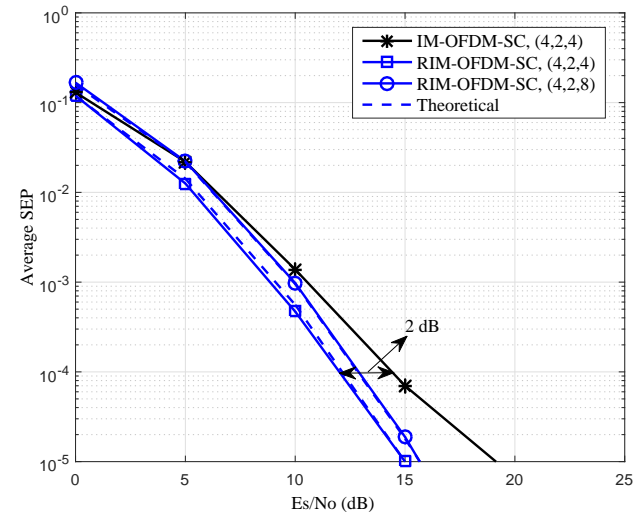


Figure 2.3: The SEP performance of RIM-OFDM-SC in comparison with IM-OFDM-SC for $N = 4$, $K = 2$, $L = 2$, $M = \{4, 8\}$.

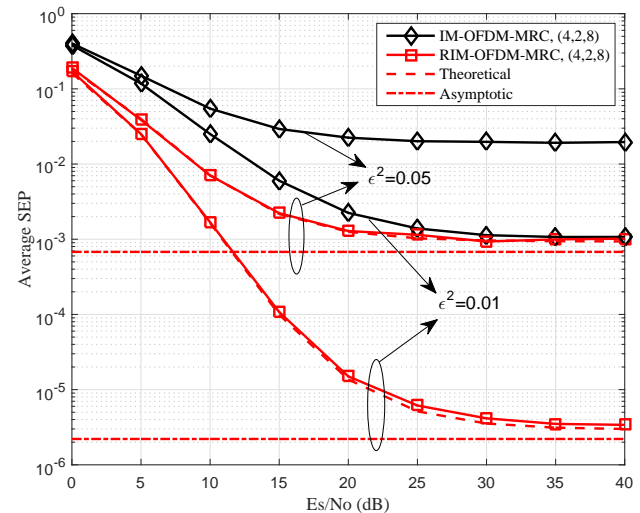


Figure 2.4: The SEP performance of RIM-OFDM-MRC in comparison with IM-OFDM-MRC under imperfect CSI when $\epsilon^2 = \{0.01, 0.05\}$.

of 10^{-4} , RIM-OFDM-MRC achieves SNR gain of about 5 dB over IM-OFDM-MRC. Analytical bounds tightly close to the simulation curves at high SNRs. This validated the performance analysis.

Fig. 2.3 compares SEP performance of RIM-OFDM-SC and that of IM-OFDM-SC. RIM-OFDM-SC achieves better SEP performance than IM-OFDM-SC. The theoretical results matches well with simulation.

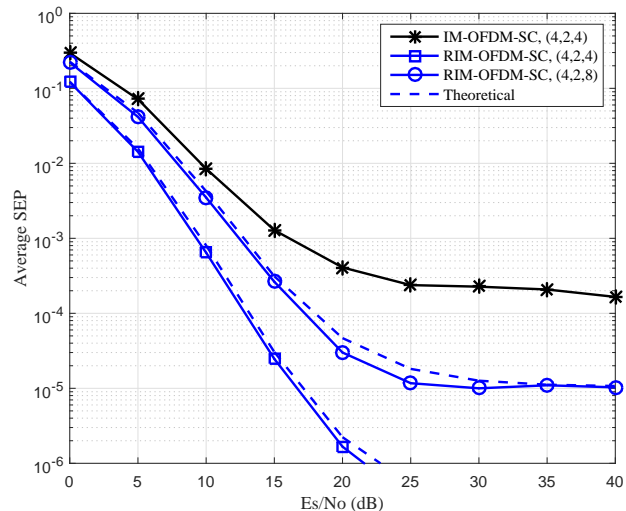


Figure 2.5: The SEP performance of RIM-OFDM-SC in comparison with IM-OFDM-SC under imperfect CSI when $\epsilon^2 = 0.01$.

Fig. 2.4 and Fig. 2.5 depict SEP of the proposed system when channel estimation errors occur at the receiver. RIM-OFDM-MRC/SC still achieves better SEP performance than that of the conventional IM-OFDM-MRC/SC. Since ϵ^2 is fixed, the error floor occurs in both cases. The analytical results tightly close to the simulation. This validates the accuracy of theoretical analysis.

2.5 Summary

This chapter proposed the RIM-OFDM-MRC/SC system which outperforms the conventional IM-OFDM-MRC/SC system at the same spectral efficiency. The system behavior of both the proposed system under different CSI conditions was investigated. The analytical and simulation results prove that the proposed scheme yields better error performance than that of the benchmark systems at the same spectral efficiency and various channel conditions.

Chapter 3

REPEATED INDEX MODULATION FOR OFDM WITH COORDINATE INTERLEAVING

3.1 RIM-OFDM-CI system model

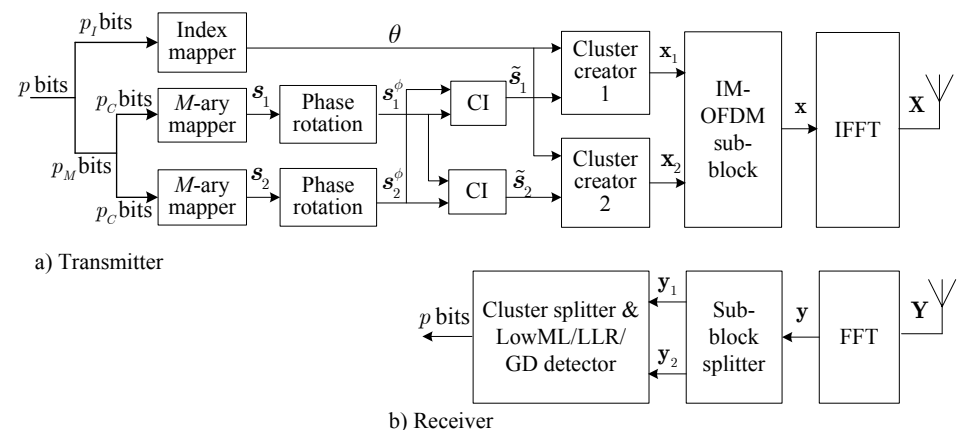


Figure 3.1: Block diagram of a typical RIM-OFDM-CI sub-block.

The block diagram of a typical RIM-OFDM-CI sub-block is depicted in Fig. 3.1. An N_F sub-carrier OFDM system is split into G sub-blocks of N_G sub-carriers. Then, each sub-block is partitioned into two clusters of N sub-carriers. Since signal processing in each sub-block is similar and independent, without loss of generality, we will focus on a typical sub-block.

Similar to the IM-OFDM system, an additional number of information bits is transferred through the indices of active sub-carriers. The remaining $N - K$ sub-carriers are set to null. Different from the conventional IM-OFDM-CI system, RIM-OFDM-CI employs the same set of active indices θ for two clusters in one sub-block as illustrated in Fig. 3.1. It is noteworthy that index repetition can improve the accuracy of the index detection over the conventional scheme at the cost of spectral efficiency. An example of the transmitted codewords in each

